Title: MAC3A and MAC3B modulate *FLM* splicing to repress photoperiod-dependent floral transition

Running Title: MAC3A and MAC3B regulate *FLM* alternative splicing to repress SD-flowering

Yu-Wen Huang[1,*†], Chih-Yen Tseng[1,2†], Yi-Tsung Tu[1], Hsin-Yu Hsieh[3],Yu-Sen Wang[1], Yun-Tung Ly[1], Yu-Zhen Chen[1], Shih-Long Tu[3], Chin-Mei Lee[1, 2, 4,5 *]

[1] Institute of Plant Biology, National Taiwan University, Taipei, 106319, Taiwan
[2] Department of Life Science, National Taiwan University, Taipei, 106319, Taiwan
[3] Institute of Plant and Microbial Biology, Academia Sinica, Taipei, 115201, Taiwan
[4] The Master Program in Global Agriculture Technology and Genomic Science, National Taiwan University, Taipei, 106319, Taiwan
[5] International Joint Degree Master's Program in Agro-biomedicine in Food and Health, National Taiwan University, Taipei, 100233, Taiwan

[†] These authors contributed equally to the article
Yu-Wen Huang (ORCID: 0009-0007-6267-8895)
Chih-Yen Tseng (ORCID: 0009-0004-1339-5213)

[*] Corresponding author:
Chin-Mei Lee (Email: chinmeilee@ntu.edu.tw; ORCID: 0009-0004-1339-5213)

Abstract

Plants adjust their flowering time by integrating environmental cues through complex regulatory networks. RNA splicing plays a crucial role in modulating gene expression in response to flowering signals. The MOS4-associated complex (MAC), consisting of the evolutionarily conserved E3 ubiquitin ligases MAC3A and MAC3B, is pivotal in splicing regulation. However, their involvement in floral transition remained unclear. This study observed that *mac3a/mac3b* mutants flowered significantly earlier under short-day (SD) conditions, a phenotype absent under long-day (LD) conditions. This early flowering correlated with upregulation of *FLOWERING LOCUS T* (*FT*) and *SUPPRESSOR OF OVEREXPRESSION OF CO 1* (*SOC1*) compared to wild-type plants. Transcriptomic analysis revealed alterations in transcript levels and splicing profiles of key floral regulators across different flowering pathways. Further investigation identified the thermosensory flowering regulator *FLOWERING LOCUS M* (*FLM*) as being influenced by *MAC3A* and *MAC3B*. Subsequently, we found that *MAC3A* and *MAC3B* exhibited higher expression and were associated with *FLM* transcripts to modulate their splicing in SD. This study elucidates how the MAC complex, through RNA splicing regulation, integrates environmental signals to modulate flowering, unveiling a new layer of complexity in flowering pathways crosstalk under non-inductive photoperiods.

Keywords

MAC3A, MAC3B, FLM, Flowering time, Alternative splicing, Photoperiod, Ambient temperature

Introduction

The floral transition from vegetative to reproductive stages represents a captivating and distinctive developmental process in angiosperms. To ensure successful reproduction, plants have evolved a sophisticated network that integrates various environmental signals, managing the plants' developmental and metabolic status to precisely control floral transition through multifaceted mechanisms (Song et al., 2015; Park et al., 2019; Gendron et al., 2021; Takagi et al., 2023). This intricate regulatory network is categorized into major pathways, including photoperiod,

age, vernalization, autonomous, thermosensory, and gibberellin (GA) pathways, with extensive crosstalk among them that warrants further exploration.

In the photoperiod pathway, the circadian clock integrates signals from the length of the day to regulate the GIGANTEA (GI)-CONSTANS (CO)-FLOWERING LOCUS T (FT) module (Imaizumi et al., 2005; Sawa et al., 2007; Takagi et al., 2023). The circadian clock orchestrates the rhythmic expression of *GIGANTEA* (*GI*), peaking before dusk. During long days (LD), light induces GI to form a complex with FLAVIN-BINDING, KELCH REPEAT, F BOX 1 (FKF1) E3 ubiquitin ligase before dusk, leading to the degradation of CYCLING DOF FACTOR1 and its homologs (CDFs), which otherwise repress *CO* transcription (Sawa et al., 2007). In LD conditions, CO protein accumulates and interacts with various transcription factors (TFs), including B and C subunits of Nuclear Factor Y, namely NF-YBs and NFYCs, to activate *FT* expression in leaves (Kumimoto et al., 2008; 2010; Cao et al., 2014). FT, functioning as a mobile florigen, moves to the shoot apical meristem (SAM), where it initiates floral transition by promoting the expression of the SAM-expressed floral integrator *SUPPRESSOR OF OVEREXPRESSION OF CO 1* (*SOC1*) and activating *LEAFY* (*LFY*) and *APETALA1* (*AP1*) (Jaeger and Wigge, 2007). Conversely, under short days (SD), the formation of the GI-FKF1 complex is reduced due to the unsynchronized accumulation of GI and FKF1 proteins, and *CO* repression by CDFs delays flowering (Sawa et al., 2007).

While extensive research has been conducted on regulating flowering time under inductive photoperiods, the mechanisms governing the repression of floral initiation in non-inductive day lengths remain largely unexplored. The GA pathway plays a significant role in suppressing the expression of *FT* and *SOC1* under SD by orchestrating multiple flowering pathways (Bao et al., 2019). GA repressor DELLA proteins interact with and stabilize the MYC3 transcription factor, which directly represses *FT* or indirectly inhibits the association of the CO/NF-YB activator with the *FT* promoter (Cao et al., 2014; Bao et al., 2019). Furthermore, GA regulates the miR156-SQUAMOSA PROMOTER BINDING PROTEIN-LIKE (SPL) module in the age flowering pathway (Huijser and Schmid, 2011). In juvenile plants, high levels of *miR156* repress *SPL9*, *SPL10*, and *SPL15*, while decreasing *miR156* levels during maturation enhances the expression of *SPL9* and its paralogs (Wang et al., 2009). SPL9 promotes the transcription of *pri-miRNA172*, which represses AP2-like TFs, including *SCHLAFMUTZE* (*SMZ*) and *EAT1 TARGETs* (*TOEs*), direct or indirect repressors of *FT* or *SOC1* (Mathieu et al., 2009). Under SD, DELLA can interact

93 with SPL9 to inhibit its activity, leading to delayed flowering (Yu et al., 2012). Moreover, DELLA
94 interacts with and stabilizes FLOWERING LOCUS C (FLC), the primary floral repressor in the
95 vernalization and autonomous pathways. FLC, along with other MADS TFs like SHORT
96 VEGETATIVE PHASE (SVP), FLOWERING LOCUS M (FLM), and its homologs, MADS
97 AFFECTING FLOWERINGs (MAFs), recruit histone modifiers to establish repressive epigenetic
98 marks on the *FT* and *SOC1* loci (Gu et al., 2013; Li et al., 2016), thereby facilitating the repression
99 of *FT* and *SOC1* by FLC.

100 Warm temperatures can alleviate the repression of flowering under SD through crosstalk
101 among flowering pathways (Fernández et al., 2016; Jin and Ahn, 2021). The bHLH transcription
102 factors PHYTOCHROME INTERACTING FACTOR 4 and 5 (PIF4 and PIF5) interact with CO
103 to promote *FT* expression at high ambient temperatures under SD (Kumar et al., 2012; Fernández
104 et al., 2016). The expression and activity of PIF4 can be enhanced by the clock/photoperiod
105 regulators EVENING COMPLEX under high-temperature conditions (Silva et al., 2020).
106 Additionally, the accessibility of PIF4 to the *FT* promoter can be regulated by the RGA DELLA
107 protein, which interacts with the DNA-binding domain of PIF4; however, the flowering regulation
108 by GA appears to be partially independent of PIF4 (de Lucas et al., 2008). Moreover, SVP and
109 FLM exert more pronounced repression of *FT* and *SOC1* expression under SD conditions
110 (Scortecci et al., 2001; Posé et al., 2013). While it has been documented that high temperatures
111 decrease the stability of the SVP protein, thereby diminishing its repressive effects on flowering
112 (Lee et al., 2013), the mechanism underlying the day-length-specific regulation of SVP-FLM
113 functions remains elusive.

114 RNA splicing emerges as a significant contributor to the modulation of florigen and
115 upstream regulators in response to environmental fluctuations (Posé et al., 2013; Shang et al., 2017;
116 Park et al., 2019; Qi et al., 2019). It generates protein isoforms from spliced RNA variants; some
117 play antagonistic roles in floral pathways, while others modulate RNA stabilities. In the
118 thermosensory flowering pathway, low and high temperatures modulate the alternative splicing of
119 *FLM* (Posé et al., 2013). The major FLM isoform, FLMβ, interacts with SVP to repress *FT* and
120 *SOC1*. Under high ambient temperatures, a decrease in *FLMβ* and an increase in *FLMδ*, which
121 leads to FLMδ protein competing with FLMβ for binding to SVP and then derepressing of *FT* and
122 *SOC1*. In a similar scenario to the photoperiod pathway, *CO* produces two isoforms in a ratio
123 determined by the photoperiods (Gil et al., 2017). COα promotes the expression of *FT*, whereas

124 COβ, encoding a truncated CO protein, interacts and negatively regulates COα by enhancing its
125 degradation by COP1. The ratios of COβ to COα are higher in SD compared to LD. Furthermore,
126 *PIF4*, another ambient-temperature-sensing flowering regulator, transcribes alternative isoforms
127 (Huang et al., 2022). PIF4-I4R (with 4th intron retained), identified as a translatable splicing
128 isoform, produces a protein that can interact with full-length PIF4, though its specific function
129 remains unknown. The significance of RNA alternative splicing in floral regulation is underscored
130 by observations that mutations in RNA splicing machinery components often lead to altered
131 flowering phenotypes (Shang et al., 2017; Park et al., 2019).

132 The RNA splicing is processed by spliceosomes, and their activities are dynamically
133 regulated by splicing factors associated with them. One such factor is the MOS4-ASSOCIATED
134 COMPLEX (MAC complex), an evolutionarily conserved splicing factor that is crucial for plant
135 RNA splicing (Monaghan et al., 2009; Jia et al., 2017; Li et al., 2019). In Arabidopsis, the MAC
136 complex consists of MAC3A and MAC3B, a pair of U-box type E3 ubiquitin ligase homologs,
137 whose C-terminal WD40 domains predicted to interact with MOS4, AtCDC5, and PRL1 as MAC
138 core proteins. The E3 ubiquitin ligase functions lie in the N-terminal U-box domains of MAC3A
139 and MAC3B to interact with E2 ubiquitin-conjugation enzyme (E2) and facilitate ubiquitin transfer
140 to their substrates. In human cells, the homolog of MAC3A and MAC3B, PRP19, not only
141 transfers ubiquitin to itself for auto-inhibition, it can ubiquitinate the K63 of PRP3, a specific
142 subunit of U4 snRNP, to enhance the association of the U4/U6/U5 snRNP within the spliceosome
143 (Song et al., 2010; de Moura et al., 2018). While the E3 ubiquitin ligase functions of MAC3A and
144 MAC3B in plants remain to be fully explored, their regulatory roles in plant RNA splicing have
145 been evidenced by transcriptome analysis, which revealed misregulation of approximately 11,000
146 genes in 9-day-old *mac3a/mac3b* double mutant seedlings (Li et al., 2019). These splicing defects
147 may explain a wide range of phenotypes, including circadian rhythm lengthening, growth
148 abnormalities, altered responses to abiotic stress, changes in defense mechanisms, and defects in
149 miRNA biogenesis (Monaghan et al., 2009; Jia et al., 2017; Tu and Chen, 2022; Jiang et al., 2023).
150 Previous reports on the flowering phenotypes under LD conditions have shown that *mac3a* and
151 *mac3b* single knockout mutants, or the *mac3a/mac3b* double knockdown mutant (the double null
152 mutant being embryonic lethal), exhibit either no differences or moderate delays in flowering (Li
153 et al., 2019; Feke et al., 2020).

154 Given the pivotal role of alternative splicing in regulating floral transitions and the
155 significant alterations of splicing events observed in the *mac3a/mac3b* Arabidopsis seedlings, the
156 previously reported phenotypes under long-day (LD) conditions cannot fully account for this
157 discrepancy (Jia et al., 2017; Li et al., 2019; Feke et al., 2020). Here, we present evidence
158 demonstrating that the Arabidopsis *mac3a/mac3b* double mutant exhibits significantly early
159 flowering under SD while displaying a phenotype similar to the wild type under LD conditions.
160 RNA-sequencing analyses of SD-grown *mac3a/mac3b* mature plants revealed expression and
161 splicing profiles of floral regulators in multiple flowering pathways that were markedly altered.
162 One potential cause for the early flowering phenotype is the involvement of *FLM*, a floral regulator
163 in the ambient temperature flowering pathway. MAC3A/MAC3B can associate with *FLM* RNA
164 to regulate the ratios of *FLMβ* and *FLMδ*, thereby influencing flowering repression. The daylength-
165 specific transcription of *MAC3A* and *MAC3B* may associated with their regulatory role in
166 flowering only under SD. These findings suggest that the MAC complex might be a central hub
167 coordinating crosstalk among the flowering pathways by regulating RNA splicing under short-day
168 conditions.
169
170 **Results**
171 ***MAC3A* and *MAC3B* repress flowering in short-day**
172 To comprehensively investigate the roles of *MAC3A* and *MAC3B* in flowering regulation,
173 we measured the flowering times under both long-day (LD, 16-hour-light/8-hour-dark) and short-
174 day (SD, 8-hour-light/16-hour-dark) conditions (**Figure 1a-b; Supplemental Table s1**). The
175 single mutants of *mac3a* and *mac3b*, as well as the *mac3a/mac3b* double mutant, displayed
176 flowering times similar to the wild type under LD, as determined by the number of rosette leaves
177 at bolting (**Figure 1a, left panel**), aligning with earlier findings by Li et al. (2019). When the
178 flowering time was assessed by the day of bolting, the *mac3a/mac3b* double mutant manifested a
179 minor delay, echoing the observations of Feke et al. (2020) (**Figure 1a, right panel**). Notably,
180 under SD conditions, the *mac3a/mac3b* double mutant exhibited significantly earlier flowering
181 based on both flowering measurement indices, opposite to phenotype in LD (**Figure 1a**). Further
182 analyses of the floral integrator transcripts, *FT* and *SOC1*, showed elevated peak expressions in
183 the *mac3a/mac3b* double mutant compared to Col-0 under SD (**Figure 1c**). This finding supports
184 early flowering phenotypes in the *mac3a/mac3b* mutant under SD.

185

186 **The flowering phenotype of *mac3a/mac3b* mutant does not correlate with *CONSTANS* levels.**

187 To ascertain if *CO* mediated the upregulation of *FT* and *SOC1* in the *mac3a/mac3b* mutant,
188 we analyzed the expression patterns of *CO*. The *CO* expression in the *mac3a* and *mac3b* single
189 mutants or *mac3a/mac3b* double mutant was comparable to Col-0 in SD or LD, respectively
190 (**Figure 2a**). Remarkably, further examination of the diurnal expression profiles of *CO* in the
191 *mac3a/mac3b* double mutant compared to wildtype under SD conditions exhibited similar patterns,
192 which did not account for the observed flowering phenotypes nor the expression of *FT* (**Figures**
193 **2b and 1b-c**). Given the roles of MAC3A and MAC3B in RNA splicing, we next investigated
194 whether these factors might influence the balance between two splice variants of *CO*, *COα* and
195 *COβ*, which in turn could modulate *FT* expression (**Figure 2c-d; Supplemental Figure s1**).
196 However, the *mac3a/mac3b* mutant presented a reduced *COα* to *COβ* ratio due to increased *COβ*
197 expression, theoretically suppressing *FT* expression. This pattern cannot explain the elevated *FT*
198 expression nor the early flowering observed in the *mac3a/mac3b* mutant in SD.

199

200 **Transcriptome analyses of *mac3a/mac3b* mutant indicate alterations in various flowering**
201 **pathways**

202 Recognizing that MAC3A and MAC3B can impact transcriptome by supporting proper
203 RNA splicing, we posited that their regulatory function in splicing might underlie the accelerated
204 flowering observed in *mac3a/mac3b* mutants under SD conditions. To test this hypothesis, we
205 performed RNA sequencing on 40-day-old SD-grown *mac3a/mac3b* mutants and wild-type plants,
206 which were still in their vegetative growth phase. The analysis revealed 605 differentially
207 expressed genes (DEGs) between the *mac3a/mac3b* mutants and Col-0 ($|\log_2(\text{fold change})| \geq 1.5$
208 and FDR$\leq$ 10%) (**Figure 3a; Supplemental Table s2**). Of these, 371 genes were upregulated,
209 while 234 were downregulated. Gene Ontology (GO) enrichment analysis of the DEGs highlighted
210 significant associations with biological processes such as circadian rhythm, response to stimulus,
211 and post-embryonic development (**Figure 3b; Supplemental Table s3**).

212 To explore the affected flowering pathways in the *mac3a/mac3b*, we compared the DEG
213 list with genes involving flowering initiation classified by Bouché et al. (2016) (**Supplemental**
214 **Table s4**). It revealed DEG across multiple flowering pathways, including circadian
215 clock/photoperiod, vernalization, age, and GA pathways in the *mac3a/mac3b* mutants (**Figure 3c**).

216 Notably, morning-phased central clock regulators, like *CCA1*, *LHY*, and *PRR9,* were upregulated,
217 whereas evening-phased regulators, such as *ELF4, LUX, TOC1*, and *PRR3,* exhibited reduced
218 expression. This shift suggests a circadian clock phase delay, aligning with the report of
219 lengthening the clock period in the *mac3a/mac3b* mutants by Feke et al. (2019). This result further
220 implies that early flowering in the *mac3a/mac3b* mutants is regulated through the CO-independent
221 pathway.

222 Investigating beyond photoperiodic influences, we found that the age and vernalization
223 pathways also experienced significant alterations (**Figure 3c**). In the age pathway, the *miRNA156*-
224 targeted flowering positive regulators, *SPL5* and *SPL15*, were downregulated and upregulated,
225 respectively. Furthermore, SPL15-regulated pri-*miRNA172*, which acts as a floral activator,
226 showed decreased transcript levels. These changes did not align with the same directions of early
227 flowering observed in the *mac3a/mac3b* mutants, suggesting the age pathway might not primarily
228 drive the phenotype. Whereas in the vernalization pathway, the floral repressor *FLC* was
229 downregulated, and the floral activator *AGL19* was upregulated. With further confirmation by RT-
230 qPCR, the *mac3a/mac3b* mutants exhibited overall lower *FLC* expression compared to the
231 wildtype under SD, and the other two MADS TFs, FLM, and SVP, which complex with FLC to
232 repress *FT*, were not significantly changed (**Supplemental Figure s2a-c**). These data suggests that
233 *MAC3A/MAC3B* partially modulates the flowering time under SD conditions through *FLC*
234 expression levels in the vernalization/autonomous pathway.

235

236 **Mutations in *MAC3A* and *MAC3B* lead to severe RNA splicing defects**

237 Given the established involvement of *MAC3A/MAC3B* in RNA splicing, prior research has
238 highlighted a marked increase in abnormal alternative splicing events, predominantly intron
239 retention, in *mac3a/mac3b* mutant seedlings (Li et al., 2019). However, the intron retention events
240 within the floral regulatory pathways remained unclear. We, therefore, investigated the alterations
241 of RNA splicing to elucidate the genetic contributors to the early flowering observed in
242 *mac3a/mac3b* mutants under SD conditions. Consequently, we identified differentially
243 alternatively spliced transcripts in our RNA-sequencing dataset with 12,031 events encoded by
244 6,836 genes differential alternative splicing events (DASs) in the *mac3a/mac3b* mutants (**Table**
245 **1**). Consistent with earlier findings, the analysis revealed that over 98% of DASs or 11,876 events
246 within 6,778 genes in the *mac3a/mac3b* mutants were characterized by increased intron retention

247 (IR) (**Table 1, Figure 4a, Supplemental Table s5**). The remaining DASs were exon skipping (ES)
248 and alterations in donor/acceptor splice sites (AltDA) involving transcription from 150 genes
249 (**Figure 4b, Table 1, Supplemental Table s6**).
250 GO analysis of the DASs showed significant enrichment of terms associated with
251 developmental processes and the RNA splicing machinery (**Figure 4c, Supplemental Table s7**).
252 Additionally, the altered RNA splicing in *mac3a/mac3b* mutants affected genes integral to primary
253 metabolic pathways, RNA processing, and responses to environmental stimuli, potentially leading
254 to the observed pleiotropic effects on flowering initiation and growth attenuation (**Figure 1b**; Li
255 et al., 2018; Li et al., 2019; Feke et al., 2020; Guo et al., 2024).
256 A subsequent comparison of genes within the DAS with established regulators of flowering
257 initiation (**Supplemental Table s4**, Bouché et al., 2016) revealed a significant overlap: 136 genes
258 from the DAS list were among the 306 known to regulate flowering (**Figure 5a; Supplemental**
259 **Tables s4-s6**). As noted, 135 of these genes exhibited upregulated retained introns in the
260 *mac3a/mac3b* mutant. These results underscore the critical role of *MAC3A/MAC3B* in
261 safeguarding splicing fidelity under SD conditions.
262
263 ***MAC3A/MAC3B* directly regulates splicing of the *FLOWERING LOCUS M* isoforms**
264 To elucidate the specific regulators whose DAS defects contribute to the upregulation of *FT*
265 and *SOC1*, and consequently the early flowering phenotype in *mac3a/mac3b* mutants, we focused
266 on identifying overlaps among the DAS gene list (**Supplemental Tables s5-s6**), known flowering
267 regulators (**Supplemental Table s4**), and potential transcription factors (TFs) upstream of the
268 DEGs (Enriched TFs in **Figure 5a, Supplemental Tables s8**). The list of potential TFs was
269 obtained by analyzing the promoter regions of each DEG for potential upstream regulators, and
270 the enriched TFs were identified based on the frequency of downstream genes present in the DEG
271 list (**Supplemental Table s8**). Among these TFs, 38 exhibited DAS, with three playing roles in
272 flowering initiation: *LHY*, *PIF4*, and *FLM* (**Figure 5a**).
273 *LHY*, a circadian clock gene acting upstream of *CO* in the photoperiod pathway, showed
274 increasing exon skipping (**Figure 5b, Supplemental Table s6**). However, our earlier findings have
275 indicated that *CO*'s alterations were not a primary factor for the early flowering observed in
276 *mac3a/mac3b* mutants. Furthermore, significant retention of the 1st and 3rd introns of *PIF4* was
277 observed in the *mac3a/mac3b* mutants (**Figure 5b, Supplemental Figure s3a, Supplemental**

278 **Table s5**). The retention of 1st intron may result in nonsense-mediated decay (NMD), while the
279 3rd intron potentially leads to truncated protein isoforms with missing or incomplete bHLH DNA
280 binding domain (**Supplemental Figure s3a-b**). Other *PIF4* alternative transcripts, though not
281 passing our selection threshold, their products may also go through NMD. Overall, it can lead to
282 less functional PIF4 proteins. Given PIF4's role as a positive regulator of *FT* as Kumar et al. (2012)
283 reported, these splicing defects could be expected to decrease *FT* expression and delay flowering.
284 Finally, *FLM*, a repressor in the thermosensory flowering pathway, exhibited increased
285 inclusion of the 3rd exon and reduced inclusion of the 2nd exon in *mac3a/mac3b* mutants (**Figures**
286 **5b and 6a, Supplemental Table s6**). The alternatively splicing patterns of *FLM* lead to two major
287 isoforms, *FLMβ* and *FLMδ*, with opposing roles in regulating flowering thermosensitivity (Posé
288 et al., 2013). *FLMδ*, characterized by the retention of the 3rd exon and exclusion of the 2nd,
289 mitigates *FLMβ*'s repression of *FT*. The ratios of the *FLMβ* to *FLMδ* decreases in *mac3a/mac3b*
290 mutants under SD conditions, which could explain the upregulation of *FT* and the consequent early
291 flowering (**Figure 6a-b, Supplemental Figure s4a**). Intriguingly, this alteration was not observed
292 under LD conditions (**Figure 6c, Supplemental Figure s4b**), indicating that *MAC3A/MAC3B*'s
293 regulation of *FLM* splicing is SD-specific. To ascertain if *MAC3A* and *MAC3B* directly influence
294 *FLM* splicing, RNA-immunoprecipitation (RIP) was performed using Arabidopsis expressing
295 FLAG-tagged *MAC3A*, revealing enrichment of *FLM* transcripts with qPCR compared to the
296 *UBQ10* control (**Figure 6d**). These findings suggest that MAC3A and MAC3B directly modulate
297 the splicing of *FLM*, adjusting the ratio of *FLMδ* to *FLMβ* to regulate flowering time under SD
298 conditions.
299
300 **Photoperiod regulates the transcript levels of *MAC3A* and *MAC3B***
301 To elucidate the specific regulatory mechanisms of *MAC3A* and *MAC3B* on flowering under
302 SD conditions, we analyzed their transcript levels under both SD and LD conditions (**Figure 7a-**
303 **b**). Notably, under SD conditions, both *MAC3A* and *MAC3B* transcripts exhibited peak expression
304 levels between 12 to 16 hours after dawn, a pattern not observed under LD conditions. These
305 photoperiod-specific expression patterns align with the changes of *FLMδ* to *FLMβ* ratios in the
306 under SD and LD (**Figures 4b-c, Supplemental Figure s4**). These findings indicate that
307 photoperiod regulates *MAC3A* and *MAC3B* transcription, which affects their function in the
308 splicing of *FLM,* potentially playing a pivotal role in modulating flowering time under SD.

309

310 **Discussion**

311 Alternative splicing critically regulates floral transition in response to environmental cues,
312 yet the underlying regulators and mechanisms remain largely unexplored (Shang et al., 2017; Park
313 et al., 2019; Qi et al., 2019). Disruptions of proteins are involved in the RNA splicing process
314 frequently result in flowering time anomalies across both LD and SD conditions. Notably,
315 mutations in U1 snRNP components, such as *RBP45d* and *PRP39a*, or the factors associated with
316 3' splicing site recognition—U2 snRNP auxiliary factors U2AF35a, U2AF35b, and U2AF65a—
317 all lead to delayed flowering in both LD and SD (Wang and Brendel, 2006; Park et al., 2019;
318 Chang et al., 2022). This study unveils the roles of MAC3A and MAC3B, key components of the
319 MOS4-associated complex (MAC) splicing factor, specifically repressing floral transition under
320 SD conditions (**Figure 8**). We discovered that the photoperiod influences *MAC3A/MAC3B*
321 expression, driving higher expression levels in SD. While transcriptome analysis suggests that
322 alterations in transcripts and splicing profiles across various flowering pathways contribute to
323 regulating flowering time, our findings specifically point to MAC3A/MAC3B's direct impact on
324 *FLM* splicing under SD conditions. Additionally, an indirect effect on *FLC* expression emerges as
325 another mechanism by which *MAC3A* and *MAC3B* suppress flowering under SD, highlighting a
326 nuanced role of alternative splicing and photoperiodic regulation in floral transition. These
327 findings also shed light on the crosstalk among floral regulatory pathways.

328

329 **MAC3A and MAC3B modulate the ratios of *FLM* isoform to regulate flowering in**
330 **response to photoperiod and temperature signals**

331 Utilizing a combination of transcriptome, RIP-qPCR, and expression analysis, we have
332 identified *FLM* as a direct splicing target of MAC3A and MAC3B under SD conditions (**Figures**
333 **5 and 6**). *FLM* functions at the crossroads of the thermosensory and autonomous flowering
334 pathways, with its splicing of isoforms modulated by temperature (Posé et al., 2013; Jin and Ahn,
335 2021). The alterations of *FLM* splicing also have been found in various splicing regulator mutants
336 under ambient temperature conditions. Our results extend this understanding by revealing that
337 *FLM* splicing is also influenced by photoperiod, suggesting a mechanism whereby *FLM* isoform
338 regulation serves as an integration point for photoperiod and temperature cues, facilitating
339 flowering in response to elevated temperatures under SD conditions. This finding offers a

340 molecular basis for previous observations of genetic interactions between *FLM-SVP* and
341 photoperiod flowering pathways (Scortecci et al., 2001). The potential for *MAC3A* and *MAC3B*
342 also respond to ambient temperatures to further integrate photoperiod and temperature signals
343 through *FLM* splicing warrants additional study.

344 Beyond *MAC3A* and *MAC3B*, the *GLYCINE-RICH RNA-BINDING PROTEINs*, *GRP7* and
345 *GRP8*, have been shown to regulate *FLM* isoform splicing (Steffen et al., 2019). GRP7
346 preferentially binds to *FLMβ* over *FLMδ* at lower temperatures under SD. The *grp7/grp8* mutants
347 exhibit reduced *FLMβ* levels, a pattern mirrored in *mac3a/mac3b* mutants alongside decreased
348 *GRP7* expression (**Figure 3c**), suggesting a collaborative role in modulating *FLMβ*. Future
349 research is poised to unravel the intricate molecular and genetic interactions between *MAC3A*,
350 *MAC3B*, and other splicing factors in adjusting *FLM* isoform ratios and orchestrating seasonal
351 flowering responses.

352

353 **The *FLC* expression may be indirectly regulated by MAC3A and MAC3B**

354 In SD conditions, the *mac3a/mac3b* mutants exhibit significantly earlier flowering, a
355 phenomenon attributed, in part, to the decreased expression of the floral repressor *FLOWERING*
356 *LOCUS C* (*FLC*) within the vernalization and autonomous pathways. This reduction in *FLC*
357 expression alleviates repression on key flowering promoters *FT* and *SOC1* (**Figures 1c,**
358 **Supplemental Figure s2a**). While the direct influence of MAC3A and MAC3B on *FLC*
359 expression appears to be limited, their role in modulating *FLC* through indirect pathways is evident,
360 particularly in the context of epigenetic regulation and post-transcriptional RNA processing
361 (Whittaker and Dean, 2017; Qi et al., 2019). *COOLAIR*, a long non-coding antisense RNA, initially
362 represses *FLC* during vernalization by altering the chromatin's H3K36me3 and H3K27me3
363 modifications (Qi et al., 2019). In the autonomous pathway, RNA processing factors further
364 regulate the *FLC* expression by the 3'-end processing of its antisense *COOLAIR* transcripts (Qi et
365 al., 2019; Whittaker and Dean, 2017). Given that *MAC3A* and *MAC3B* have been established to
366 impact miRNA biosynthesis (Li et al., 2018), their potential effect on *COOLAIR* processing and,
367 consequently, on *FLC* expression in *mac3a/mac3b* mutants warrants further investigation.

368 Additionally, transcriptome analysis revealed changes in *GRP7* expression, a known
369 interactor with *COOLAIR*, suggesting a possible regulatory link between *MAC3A*, *MAC3B*, *GRP7*,
370 and *FLC* expression (**Figure 3c**) (Xiao et al., 2015). Interestingly, the regulatory dynamics of

371 *MAC3A/MAC3B* and *GRP7* diverge; *MAC3A/MAC3B* seem to specifically influence *FLC*
372 expression under SD, contrasting with *GRP7*'s broader regulatory scope across photoperiods (Xiao
373 et al., 2015; Steffen et al., 2019). Despite *GRP7* being downregulated in *mac3a/mac3b* mutants,
374 this does not mask the *mac3a/mac3b* early flowering phenotype (**Figures 1a, 3c**). This suggests
375 that under SD, MAC3A and MAC3B are crucial for maintaining *FLC* expression, potentially
376 gating the autonomous flowering pathway and highlighting a nuanced role in flowering regulation.
377

378 **Potential versatile molecular functions of MAC3A and MAC3B in regulating flowering**

379 MAC3A and MAC3B are bona fide U-box-containing E3 ubiquitin ligases that auto-
380 ubiquitinate themselves or other substrates (Li et al., 2018; Guo et al., 2024; Yu et al., 2024). The
381 functions of E3 ubiquitin ligases are crucial for modulating various biological processes, including
382 miRNA biogenesis, lateral root emergence, and organ size control. However, whether the E3
383 functions are required for their role in SD-specific flowering time regulation remains to be
384 explored. In human cells, the homologs of MAC3A and MAC3B, PRP19, have been shown to
385 ubiquitinate spliceosome subunits, affecting their assembly and activities (Song et al., 2010; de
386 Moura et al., 2018;). This suggests that the E3 ubiquitin ligase functions of MAC3A and MAC3B
387 might be vital for regulating splicing in the flowering pathways. Furthermore, in addition to their
388 role as E3 ubiquitin ligases, MAC3A and MAC3B have been reported to interact with histone
389 modifiers such as HISTONE DEACETYLASE 15 (HDA15) (Tu and Chen et al., 2022). Moreover,
390 recent findings indicate that MAC3A and MAC3B associate with cryptochromes or other proteins
391 to form biomolecular condensates in the nucleus under specific conditions, suggesting a potential
392 role in regulating gene expression through epigenetic or transcriptional mechanisms beyond RNA
393 splicing (Li et al., 2018; Jia et al., 2023).
394

395 **Materials and Methods**

396 **Plant Materials and Growth Conditions**

397 All *Arabidopsis thaliana* lines utilized in this study were derived from the Columbia-0 (Col-0)
398 genetic background. The *mac3a* (SALK_089300), *mac3b* (SALK_050811), and the *mac3a/mac3b*
399 double mutants (CS69985) were as characterized by Monaghan et al. (2009). All mutant lines were
400 obtained from the Arabidopsis Biological Resource Center (ABRC) and confirmed through
401 genotyping and PCR.

402

403 Seed stratification was performed by soaking in sterilized water at 4°C for three days in darkness,
404 followed by sowing on the soil. For seedlings grown on plates, seeds underwent sterilization with
405 70% ethanol and 0.1% TRITON® X-100, then were plated on 1/2 strength Murashige and Skoog
406 (MS) medium (Caisson, Cat# MSP02) supplemented with 0.8% agar (Duchefa Biochemie, Cat#
407 P1003). Plates were kept at 4°C in the dark for three days before being moved to growth chambers.
408 Growth conditions for plants, whether in soil or on plates, included long-day (LD) conditions (16
409 hours of light/8 hours of dark) or short-day (SD) conditions (8 hours of light/16 hours of dark),
410 maintained at 22°C with light intensities ranging from 85 to 120 μmol m^{-2} s^{-1}.
411

412 Flowering time was quantitatively assessed using two metrics: the date of flowering, when the
413 inflorescence stem reached a length of 1 cm, and the total leaf count, recorded once the
414 inflorescence stem achieved a length of 7 cm. Each experimental replicate comprised 15-20 plants
415 per genetic line.
416

417 **Reverse Transcription Quantitative PCR (RT-qPCR)**

418 To quantify RNA expression, *Arabidopsis thaliana* seedlings grown for 10 days under LD
419 conditions and 14 days under SD conditions were harvested. The harvested seedlings were flash-
420 frozen in liquid nitrogen and ground into a fine powder using a ball grinder (Retsch, MM400).
421 Total RNA was then extracted from the tissue powder using TRIzol Reagent (Invitrogen, Cat#
422 15596-018) following the manufacturer's instructions. DNase treatment (Promega, Cat# M6101)
423 was applied to the extracted RNA samples to eliminate potential DNA contamination. Finally, the
424 RNA concentrations and 260/280 ratios were measured with NanoDrop One (ThermoFisher)
425 before frozen storage of the RNA samples.
426

427 For reverse transcription, 1000 ng of DNase-treated RNA was used in a 20 μL reaction employing
428 oligo-dT primers and random hexamers according to the protocol provided by Takara (Cat#
429 RR014B). The relative expression levels of the target genes were assessed via qPCR. For this, 4
430 μL of 10-fold diluted cDNA was combined with 5 μL of iQ SYBR Green Supermix (Bio-Rad,
431 Cat# 170-8880) and 0.5 μL of each 10 μM forward and reverse primers, bringing the total reaction

volume to 10 µL. These qPCR reactions were conducted using the CFX Connect Real-Time System (Bio-Rad) following a three-step PCR protocol.

This study incorporated three biological replicates for each qPCR experiment. Expression levels were normalized to the internal control gene *UBQ10* (AT4G05320). The sequences of all primers used for RT-qPCR are provided in **Supplemental Table s9**.

RNA-sequencing Analyses of Differentially Expressed Genes (DEG) and Differential Alternative Spliced (DAS) Events

Leaves from 40-day-old Col-0 and *mac3a/mac3b* mutants grown on the soil under SD conditions were collected at Zeitgeber time 8 (ZT8). Total RNA was extracted using the RNeasy Plant Mini Kit (QIAGEN, Cat# 74904), with subsequent removal of genomic DNA contamination employing the RNase-Free DNase Set (QIAGEN, Cat# 79254). RNA-sequencing (RNA-seq) libraries for triple replicates were prepared utilizing the Illumina TruSeq toolkit (Illumina, Cat# FC-122-1001). The detailed pipelines of differential gene expression (DEG) analysis and differential alternative splicing (DAS) event detection are provided in **Supplemental Method s1**.

Gene Ontology (GO) annotations for DEGs and DAS genes (**Supplemental Tables s3 and s7**) were analyzed using the g:GOst feature on the g:Profiler website (https://biit.cs.ut.ee/gprofiler/gost; Raudvere et al., 2019) for enriched GO terms. This study used the calculation method published by Storey and Tibshirani (2003) to estimate the FDR. Data visualization was accomplished with the ggplot2 package in R (Wickham, 2016).

To identify key transcription factors (TFs) implicated in the *mac3a/mac3b* mutants (**Supplemental Table s8**), we performed TF enrichment analysis on the differentially expressed gene (DEG) lists (**Supplemental Table s2**) utilizing the FunTFBS interaction list with a cutoff p-value of <0.05 (PlantRegMap, http://plantregmap.gao-lab.org/tf_enrichment.php; Tian et al., 2020). The FunTFBS interaction list was pre-generated based on a significant Pearson correlation between binding motif frequencies and conservation scores across base pairs. TFs with at least one FunTFBS present on the differentially expressed genes were included in the TF enrichment analysis. Fisher's exact tests were then conducted to identify TFs with significantly over-

463 represented target genes within the input gene set, compared to their binding sites in the genomic
464 background.
465
466 **Generation of *FLAG-MAC3A*-overexpressing Transgenic Arabidopsis**
467 To construct *35S::6xHis-3xFLAG-MAC3A* (or called *FLAG-MAC3A*-overexpression lines) in the
468 *mac3a/mac3b* or *mac3a* mutant background, the *MAC3A* coding sequence was subcloned into the
469 *pB7-HFN* plant binary vector. This vector was then transformed into *Agrobacterium tumefaciens*
470 strain *GV3101*, which was used to introduce the construct into the *mac3a/mac3b* double mutant
471 using the floral dip method. Selection of homozygous T3 plants was performed by screening on
472 1/2 MS medium supplemented with 10 µg/mL glufosinate ammonium (Cyrusbiosciences, Cat#
473 101-77182-82-2).
474
475 **RNA-Immunoprecipitation Quantitative PCR (RIP-qPCR)**
476 RNA immunoprecipitation (RIP) was conducted on 15-day-old *mac3a/mac3b* and MAC3A-
477 FLAG-overexpression *Arabidopsis* seedlings harvested at ZT12, following a modified protocol
478 from Terzi and Simpson (2009). Seedlings were cross-linked with 1% formaldehyde under vacuum
479 infiltration for 20 minutes, with the reaction quenched using 200 mM glycine for an additional 5
480 minutes under vacuum. After four washes with ddH2O and drying, the samples were frozen in
481 liquid nitrogen and pulverized.
482
483 The pulverized tissue was incubated in 30 mL of buffer 1 (400 mM sucrose, 10 mM Tris-HCl pH
484 8.0, 10 mM $MgCl_2$, 5 mM β-mercaptoethanol, 1 mM PMSF, 1× Roche cOmplete EDTA-free
485 Protease Inhibitor Cocktail, and 50 U/mL Invitrogen™ SUPERase•In™ RNase Inhibitor) on ice
486 for 30 minutes. Following filtration through miracloth and centrifugation at 3000 g for 30 minutes
487 at 4°C, the pellet was resuspended in buffer 2 (250 mM sucrose, 10 mM Tris-HCl pH 8.0, 10 mM
488 $MgCl_2$, 5 mM β-mercaptoethanol, 1 mM PMSF, 1× cOmplete EDTA-free Protease Inhibitor
489 Cocktail, and 50 U/mL SUPERase•In™ RNase Inhibitor), then centrifuged at 12000 g for 10
490 minutes at 4°C. The subsequent pellet was suspended in buffer 3 (1.7 M sucrose, 10 mM Tris-HCl
491 pH 8.0, 2 mM $MgCl_2$, 5 mM β-mercaptoethanol, 1 mM PMSF, 1× cOmplete EDTA-free Protease
492 Inhibitor Cocktail, and 50 U/mL SUPERase•In™ RNase Inhibitor), centrifuged at 16000 g for 20
493 minutes at 4°C, and the resulting nuclei pellets were resuspended in buffer 4 (50 mM Tris-HCl pH

494 8.0, 10 mM EDTA pH8.0, 1% SDS, 1 mM PMSF, 1× cOmplete EDTA-free Protease Inhibitor
495 Cocktail, and 160 U/mL SUPERase•In™ RNase Inhibitor) for 10 minutes on ice. Nucleic acids
496 were fragmented using a Branson Digital Sonifier SFX 250, with a cycle of 15 minutes on and 1
497 minute off, repeated 20 times (totaling 5 minutes), followed by centrifugation at 15000 g for 10
498 minutes at 4°C.
499
500 The nuclear extract was then diluted with RIP dilution buffer (16.7 mM Tris-HCl pH 8.0, 1.2 mM
501 EDTA pH8.0, 167 mM NaCl, 0.5% Triton X-100, 1 mM PMSF, 1× cOmplete EDTA-free Protease
502 Inhibitor Cocktail, and 160 U/mL SUPERase•In™ RNase Inhibitor) and incubated with anti-
503 FLAG® antibody magnetic beads (Merck, Cat# M8823) overnight at 4°C with gentle rotation.
504 Beads were washed four times in RIP wash buffer (50 mM Tris-HCl pH 8.0, 10 mM EDTA pH8.0,
505 300 mM NaCl, 0.5% Triton X-100, 0.1 % SDS, 1 mM PMSF, 1× cOmplete EDTA-free Protease
506 Inhibitor Cocktail, and 40 U/mL SUPERase•In™ RNase Inhibitor) and treated with proteinase K
507 (Sigma, Cat# p2308). RNA was extracted using TRIzol reagent (Invitrogen, Cat# 15596-018), and
508 residual genomic DNA was removed with RQ1 RNase-free DNase (Promega, Cat# M6101). The
509 qPCR procedures were described as RT-qPCR section with the primers listed in **Supplemental**
510 **Table s9.**
511
512 **Protein Extraction and Immunoblot**
513 Protein was extracted from *Arabidopsis thaliana* seedlings, previously ground to a powder using
514 a freezer mill (Retsch, MM400) in liquid nitrogen. The extraction buffer contained 4 M Urea, 100
515 mM Tris-HCl (pH 6.8), 5% SDS, 15% Glycerol, supplemented with 0.4% protease inhibitor
516 cocktail (Roche, Cat# 04693132001), 0.5% β-mercaptoethanol (PanReac AppliChem, Cat#
517 A11080100), and 0.2% bromophenol blue dye (Sigma, Cat# 62625289). Samples were
518 subsequently boiled for 5 minutes at 105°C, followed by centrifugation at 13,000 g for 5 minutes
519 to collect the supernatant. The clarified protein extracts were either analyzed immediately or stored
520 at -80°C.
521
522 For immunoblot analysis, around 5 μg of the protein samples were subjected to 10% SDS-PAGE
523 for separation. Proteins were then transferred to PVDF membranes (Millipore, Cat# IPVH00010)
524 at 4°C. The membranes were blocked with 5% non-fat milk in TBST buffer (20 mM Tris-base,

525 150 mM NaCl, 0.1% Tween 20) for 1 hour at room temperature, followed by overnight incubation
526 at 4°C with a 1:5000 dilution of anti-FLAG antibody (Sigma, Cat# F1804) in the blocking solution.
527 After washing thrice with TBST, the membranes were incubated with an HRP-conjugated
528 secondary antibody (Promega, Cat# W4021, 1:10,000 dilution) in blocking solution, washed three
529 times in TBST, and developed using Clarity Western ECL Substrate (Bio-Rad, Cat# 1705061) for
530 imaging on a 5200 Chemiluminescent Imaging System (Tanon). This procedure was
531 independently replicated with three biological samples.
532
533 **Statistical analysis**
534 Statistical analysis for experiments was performed using the software Graphpad Prism 10.
535 Student's t-test, one-way ANOVA (non-parametric Kruskal-Wallis test), or two-way ANOVA
536 were adopted. The P values of post-hoc tests used are individually indicated in the figures. For
537 one-way ANOVA and two-way ANOVA, P values were used to indicate significant differences
538 between multiple groups with Dunn's or Šídák's post-hoc statistical test, respectively (ns, no
539 significant difference; *, $P< 0.05$; **, $P< 0.01$; ***, $P< 0.001$). Each experiment was performed
540 with at least three biological replicates. The results are presented as mean values ± standard error
541 of the mean (SE).
542
543
544 **List of supplemental data**
545 **Supplemental Table s1.** The flowering time was measured by rosette leaf number and bolting day
546 in the Col-0, *mac3a*, *mac3b*, and *mac3a/mac3b* mutants grown under LD (16h light/8h dark) or
547 SD (8h light/16h dark).
548 **Supplemental Table s2.** The list of differentially expressed genes (DEG) in the *mac3a/mac3b*
549 mutant under SD compared to Col-0.
550 **Supplemental Table s3.** The results of gene ontology (GO) analyses of DEG in the *mac3a/mac3b*
551 mutant.
552 **Supplemental Table s4.** The list of the flowering regulators classified by Bouché et al. (2016).
553 **Supplemental Table s5.** The list of differentially alternative spliced (DAS) events belongs to the
554 intron retention (IR) category in the *mac3a/mac3b* mutant under SD compared to Col-0 in SD.

555 **Supplemental Table s6.** The list of differentially alternative spliced (DAS) events belongs to exon
556 skipping (DES) and alternative donor/acceptor sites (AltDA) categories in the *mac3a/mac3b*
557 mutant under SD compared to Col-0 under SD.
558 **Supplemental Table s7.** The gene ontology (GO) analyses of DAS in the *mac3a/mac3b* mutant
559 in SD.
560 **Supplemental Table s8.** The list of enriched transcription factors (TFs) from the promoter
561 analysis of DEG in the *mac3a/mac3b* mutant.
562 **Supplemental Table s9.** List of primers used in this study.
563 **Supplemental Figure s1.** The expression of *CO* isoforms in SD measured by RT-qPCR
564 **Supplemental Figure s2.** The expression of *FLC*, *FLM*, and *SVP* in SD measured by RT-qPCR
565 **Supplemental Figure s3.** Alternatively spliced events of *PIF4* were identified in the
566 *mac3a/mac3b* mutant
567 **Supplemental Figure s4.** The diurnal expression profiles of *FLM* isoforms in LD and SD
568 **Supplemental Method s1.** RNA-sequencing Analyses of Differentially Expressed Genes (DEG)
569 and Differential Alternative Spliced (DAS) Events
570
571 **Acknowledgments**
572 We thank Dr. Shu-Hsing Wu, Dr. Huang-Lung Tsai, Dr. Ming-Jung Liu, and Dr. Mei-Chun Cheng
573 for valuable discussion. We also thank Shu-Jen Chou in the Genomic Technology Core Laboratory
574 and Wen-Dar Lin at the Bioinformatics Core Laboratory of the Institute of Plant and Microbial
575 Biology, Academia Sinica, for technical assistance. We also thank the excellent technical
576 assistance and the facilities of Technology Commons, College of Life Science, National Taiwan
577 University.
578
579 **Author Contributions**
580 The study was conceptualized, and the manuscript was written by C.M.L., Y.W.H., and C.Y.T..
581 Y.W.H., C.Y.T., and Y.T.T. designed and executed the experiments. S.L.T., H.Y.H., and C.Y.T.
582 analyzed the RNA-sequencing data. Y.S.W., Y.Z.C., and Y.T.L. prepared the materials and
583 conducted the experiments.
584
585 **Conflict of Interest**

586 The authors declare that the research was conducted in the absence of any commercial or financial
587 relationships that could be construed as a potential conflict of interest.
588
589 **Data availability**
590 The sequencing data generated in this study have been deposited into GEO with a code: GSE
591 261591.
592
593 **Funding**
594 C.M.L.: NSTC-110-2311-B-002-025-, NSTC-111-2311-B-002-025-, NSTC-112-2311-B-002-
595 025-, NTU-CC-110L893604, NTU-CC-111L893004, and NTU-CC-112L891804
596 S.L.T.: NSTC-111-2311-B-001-004-, NSTC-112-2311-B-001-004-
597 C.Y.T.: NSTC-112-2813-C-002-208-B, PhD fellowship from NSTC and NTU
598 Y.T.T.: NTU-CC-111L4000, NTU-CC-112L4000, NTU-CC-113L4000
599 Y.S.W.: MOE Industry-Academia Cooperative PhD fellowship
600
601 **References**
602 **Bao S, Hua C, Huang G, Cheng P, Gong X, Shen L, Yu H.** (2019) Molecular Basis of Natural
603 Variation in Photoperiodic Flowering Responses. Developmental Cell **50**(1), 90-101.
604 **Bouché F, Lobet G, Tocquin P, Périlleux C.** (2016) FLOR-ID: an interactive database of
605 flowering-time gene networks in Arabidopsis thaliana. Nucleic Acids Research **44**(D1),
606 D1167-1171.
607 **Cao S, Kumimoto RW, Gnesutta N, Calogero AM, Mantovani R, Holt BF.** (2014) A distal
608 CCAAT/NUCLEAR FACTOR Y complex promotes chromatin looping at the FLOWERING
609 LOCUS T promoter and regulates the timing of flowering in Arabidopsis. Plant Cell **26**(3),
610 1009-1017.
611 **Chang P, Hsieh HY, Tu SL.** (2022) The U1 snRNP component RBP45d regulates temperature-
612 responsive flowering in Arabidopsis. Plant Cell **34**(2), 834-851.
613 **de Lucas M, Davière JM, Rodríguez-Falcón M, Pontin M, Iglesias-Pedraz JM, Lorrain S,**
614 **Fankhauser C, Blázquez MA, Titarenko E, Prat S.** (2008) A molecular framework for
615 light and gibberellin control of cell elongation. Nature **451**(7177), 480-484.

616 **de Moura TR, Mozaffari-Jovin S, Szabó CZK, Schmitzová J, Dybkov O, Cretu C, Kachala**
617 **M, Svergun D, Urlaub H, Lührmann R, Pena V.** (2018) Prp19/Pso4 Is an Autoinhibited
618 Ubiquitin Ligase Activated by Stepwise Assembly of Three Splicing Factors. Molecular Cell
619 **69**(6), 979-992.
620 **Feke A, Liu W, Hong J, Li MW, Lee CM, Zhou EK, Gendron JM.** (2019) Decoys provide a
621 scalable platform for the identification of plant E3 ubiquitin ligases that regulate circadian
622 function. eLife **8**, e44558.
623 **Feke AM, Hong J, Liu W, Gendron JM.** (2020) A Decoy Library Uncovers U-Box E3 Ubiquitin
624 Ligases That Regulate Flowering Time in Arabidopsis. Genetics **215**(3), 699-712.
625 **Fernández V, Takahashi Y, Le Gourrierec J, Coupland G.** (2016) Photoperiodic and
626 thermosensory pathways interact through CONSTANS to promote flowering at high
627 temperature under short days. Plant Journal **86**(5), 426-440.
628 **Gendron JM, Leung CC, Liu W.** (2021) Energy as a seasonal signal for growth and reproduction.
629 Current Opinion in Plant Biology **63**, 102092.
630 **Gil KE, Park MJ, Lee HJ, Park YJ, Han SH, Kwon YJ, Seo PJ, Jung JH, Park CM.** (2017)
631 Alternative splicing provides a proactive mechanism for the diurnal CONSTANS dynamics
632 in Arabidopsis photoperiodic flowering. Plant Journal **89**, 128-140.
633 **Gu X, Le C, Wang Y, Li Z, Jiang D, Wang Y, He Y.** (2013) Arabidopsis FLC clade members
634 form flowering-repressor complexes coordinating responses to endogenous and
635 environmental cues. Nature Communications **4**, 1947.
636 **Guo X, Zhang X, Jiang S, Qiao X, Meng B, Wang X, Wang Y, Yang K, Zhang Y, Li N Chen**
637 **T, Kang Y, Yao M, Zhang X, Wang X, Zhang E, Li J, Yan D, Hu Z, Botella JR, Song**
638 **CP, Li Y, Guo S.** (2024) E3 ligases MAC3A and MAC3B ubiquitinate UBIQUITIN-
639 SPECIFIC PROTEASE14 to regulate organ size in Arabidopsis. Plant Physiology **194**(2),
640 684-697.
641 **Huang CK, Lin WD, Wu SH.** (2022) An improved repertoire of splicing variants and their
642 potential roles in Arabidopsis photomorphogenic development. Genome Biology **23**(1), 50.
643 **Huijser P, Schmid M.** (2011) The control of developmental phase transitions in plants.
644 Development **138**(19), 4117-4129.

645 **Imaizumi T, Schultz TF, Harmon FG, Ho LA, Kay SA.** (2005) FKF1 F-box protein mediates
646 cyclic degradation of a repressor of CONSTANS in Arabidopsis. Science **309**(5732), 293-
647 297.
648 **Jin S, Ahn JH.** (2021) Regulation of flowering time by ambient temperature: repressing the
649 repressors and activating the activators. New Phytologist **230**(3), 938-942.
650 **Jia M, Chen X, Shi X, Fang Y, Gu Y.** (2023) Nuclear transport receptor KA120 regulates
651 molecular condensation of MAC3 to coordinate plant immune activation. Cell Host &
652 Microbe **31**(10), 1685-1699.e7.
653 **Jia T, Zhang B, You C, Zhang Y, Zeng L, Li S, Johnson KCM, Yu B, Li X, Chen X.** (2017)
654 The Arabidopsis MOS4-Associated Complex Promotes MicroRNA Biogenesis and Precursor
655 Messenger RNA Splicing. Plant Cell **29**(10):2626-2643.
656 **Jiang B, Zhong Z, Su J, Zhu T, Yueh T, Bragasin J, Bu V, Zhou C, Lin C, Wang X.** (2023)
657 Co-condensation with photoexcited cryptochromes facilitates MAC3A to positively control
658 hypocotyl growth in Arabidopsis. Science Advances **9**(32), eadh4048.
659 **Jaeger KE, Wigge PA.** (2007) FT protein acts as a long-range signal in Arabidopsis. Current
660 Biology **17**(12), 1050-1054.
661 **Kumar SV, Lucyshyn D, Jaeger KE, Alós E, Alvey E, Harberd NP, Wigge PA.** (2012)
662 Transcription factor PIF4 controls the thermosensory activation of flowering. Nature
663 **484**(7393), 242-245.
664 **Kumimoto RW, Adam L, Hymus GJ, Repetti PP, Reuber TL, Marion CM, Hempel FD,**
665 **Ratcliffe OJ.** (2008) The Nuclear Factor Y subunits NF-YB2 and NF-YB3 play additive roles
666 in the promotion of flowering by inductive long-day photoperiods in Arabidopsis. Planta
667 **228**(5), 709-723.
668 **Kumimoto RW, Zhang Y, Siefers N, Holt BF 3rd.** (2010) NF-YC3, NF-YC4 and NF-YC9 are
669 required for CONSTANS-mediated, photoperiod-dependent flowering in Arabidopsis
670 thaliana. Plant Journal **63**(3), 379-391.
671 **Lee JH, Ryu HS, Chung KS, Posé D, Kim S, Schmid M, Ahn JH.** (2013) Regulation of
672 temperature-responsive flowering by MADS-box transcription factor repressors. Science
673 **342**(6158), 628-632.
674 **Li M, An F, Li W, Ma M, Feng Y, Zhang X, Guo H.** (2016) DELLA proteins interact with FLC
675 to repress flowering transition. Journal of Integrative Plant Biology **58**(7), 642-655.

676 **Li S, Liu K, Zhou B, Li M, Zhang S, Zeng L, Zhang C, Yu B.** (2018) MAC3A and MAC3B,
677 Two Core Subunits of the MOS4-Associated Complex, Positively Influence miRNA
678 Biogenesis. Plant Cell **30**, 481-494.
679 **Li Y, Yang J, Shang X, Lv W, Xia C, Wang C, Feng J, Cao Y, He H, Li, Ma L.** (2019) SKIP
680 regulates environmental fitness and floral transition by forming two distinct complexes in
681 Arabidopsis. New Phytologist **224**(1), 321-335.
682 **Mathieu J, Yant LJ, Mürdter F, Küttner F, Schmid M.** (2009) Repression of flowering by the
683 miR172 target SMZ. PLOS Biology **7**(7), e1000148.
684 **Monaghan J, Xu F, Gao M, Zhao Q, Palma K, Long C, Chen S, Zhang Y, Li X.** (2009) Two
685 Prp19-like U-box proteins in the MOS4-associated complex play redundant roles in plant
686 innate immunity. PLOS Pathogens **5**, e1000526.
687 **Park YJ, Lee JH, Kim JY, Park CM.** (2019) Alternative RNA Splicing Expands the
688 Developmental Plasticity of Flowering Transition. Frontiers in Plant Science **10**, 606.
689 **Posé D, Verhage L, Ott F, Yant L, Mathieu J, Angenent GC, Immink RG, Schmid M.** (2013)
690 Temperature-dependent regulation of flowering by antagonistic FLM variants. Nature **503**,
691 414-417.
692 **Raudvere U, Kolberg L, Kuzmin I, Arak T, Adler P, Peterson H, Vilo J.** (2019) g:Profiler: a
693 web server for functional enrichment analysis and conversions of gene lists (2019 update).
694 Nucleic Acids Research **47**(W1), W191-198.
695 **Qi HD, Lin Y, Ren QP, Wang YY, Xiong F, Wang XL.** (2019) RNA Splicing of FLC Modulates
696 the Transition to Flowering. Frontiers in Plant Science **10**, 1625.
697 **Sawa M, Nusinow DA, Kay SA, Imaizumi T.** (2007) FKF1 and GIGANTEA complex formation
698 is required for day-length measurement in Arabidopsis. Science **318**(5848), 261-265.
699 **Scortecci KC, Michaels SD, Amasino RM.** (2001) Identification of a MADS-box gene,
700 FLOWERING LOCUS M, that represses flowering. Plant Journal **26**(2), 229-236.
701 **Shang X, Cao Y, Ma L.** (2017) Alternative Splicing in Plant Genes: A Means of Regulating the
702 Environmental Fitness of Plants. International Journal of Molecular Sciences **18**(2), 432.
703 **Silva CS, Nayak A, Lai X, Hutin S, Hugouvieux V, Jung JH, López-Vidriero I, Franco-**
704 **Zorrilla JM, Panigrahi KCS, Nanao MH, Wigge PA, Zubieta C.** (2020) Molecular
705 mechanisms of evening complex activity in Arabidopsis. PANS **117**(12), 6901-6909.

706 **Song EJ, Werner SL, Neubauer J, Stegmeier F, Aspden J, Rio D, Harper JW, Elledge SJ,**
707 **Kirschner MW, Rape M.** (2010) The Prp19 complex and the Usp4Sart3 deubiquitinating
708 enzyme control reversible ubiquitination at the spliceosome. Genes & Development **24**, 1434-
709 1447.
710 **Song YH, Shim JS, Kinmonth-Schultz HA, Imaizumi T.** (2015) Photoperiodic flowering, time
711 measurement mechanisms in leaves. Annual Review of Plant Biology **66**, 441-464.
712 **Steffen A, Elgner M, Staiger D.** (2019) Regulation of Flowering Time by the RNA-Binding
713 Proteins AtGRP7 and AtGRP8. Plant and Cell Physiology **60(9)**, 2040-2050.
714 **Storey JD, Tibshirani R.** (2003) Statistical significance for genomewide studies. PNAS **100**(16),
715 9440-9445.
716 **Takagi H, Hempton AK, Imaizumi T.** (2023) Photoperiodic flowering in Arabidopsis:
717 Multilayered regulatory mechanisms of CONSTANS and the florigen FLOWERING LOCUS
718 T. Plant Communications **4(3)**, 100552.
719 **Terzi LC, Simpson GG. (**2009) Arabidopsis RNA immunoprecipitation. Plant Journal **59**(1), 163-
720 168.
721 **Tian F, Yang DC, Meng YQ, Jin J, Gao G.** (2020) PlantRegMap: charting functional regulatory
722 maps in plants. Nucleic Acids Research **48**(D1), D1104-1113.
723 **Tu YT, Chen CY, Huang YS, Chang CH, Yen MR, Hsieh JA, Chen PY, Wu K.** (2022)
724 HISTONE DEACETYLASE 15 and MOS4-associated complex subunits 3A/3B coregulate
725 intron retention of ABA-responsive genes. Plant Physiology **190**(1), 882-897.
726 **Wang BB, Brendel V.** (2006) Molecular characterization and phylogeny of U2AF35 homologs
727 in plants. Plant Physiology **140**(2), 624-636.
728 **Wang JW, Czech B, Weigel D.** (2009) miR156-regulated SPL transcription factors define an
729 endogenous flowering pathway in Arabidopsis thaliana. Cell **138(4)**, 738-749.
730 **Whittaker C, Dean C.** (2017) The FLC Locus: A Platform for Discoveries in Epigenetics and
731 Adaptation. Annual Review of Cell and Development Biology **33,** 555-575.
732 **Wickham H.** (2016) ggplot2: Elegant Graphics for Data Analysis. Springer-Verlag New York.
733 ISBN 978-3-319-24277-4.
734 **Xiao J, Li C, Xu S, Xing L, Xu Y, Chong K.** (2015) JACALIN-LECTIN LIKE1 Regulates the
735 Nuclear Accumulation of GLYCINE-RICH RNA-BINDING PROTEIN7, Influencing the

736 RNA Processing of FLOWERING LOCUS C Antisense Transcripts and Flowering Time in
737 Arabidopsis. Plant Physiology **169**(3), 2102-2117.
738 **Yu S, Galvão VC, Zhang YC, Horrer D, Zhang TQ, Hao YH, Feng YQ, Wang S, Schmid M,**
739 **Wang JW.** (2012) Gibberellin regulates the Arabidopsis floral transition through miR156-
740 targeted SQUAMOSA promoter binding-like transcription factors. Plant Cell **24**(8), 3320-
741 3332.
742 **Yu Z, Qu X, Lv B, Li X, Sui J, Yu Q, Ding Z.** (2024) MAC3A and MAC3B mediate degradation
743 of the transcription factor ERF13 and thus promote lateral root emergence. Plant Cell,
744 koae047.

Table 1. The differentially alternative spliced (DAS) events in the *mac3a/mac3b* mutant compared to Col-0 under SD

The number of DAS events, including intron retention (IR), exon skipping (ES), alternative donor/acceptor splicing site (AltDA), and their corresponding gene number was listed. The IR, AltDA, or ES events were identified by the Chi-square test of reads with or without IR, AltDA, or ES in between Col-0 and *mac3a/mac3b* mutants, respectively. Out of the identified alternative splicing events, the differentially alternative splicing events were selected by significance and fold-change among replicates. The false discovery rate (FDR) of accepted p-values is limited to 5%. The list of genes and events is provided in Supplemental Tables s5 and s6.

	***mac3a/mac3b* v.s. WT**			
	Events	**%**	**Genes**	**%**
total	**12031**	**100.00**	**6836**	**100.00**
IR	**11876**	**98.71**	**6778**	**99.15**
ES	**150**	**1.24**	**146**	**2.14**
AltDA	**5**	**0.04**	**4**	**0.06**

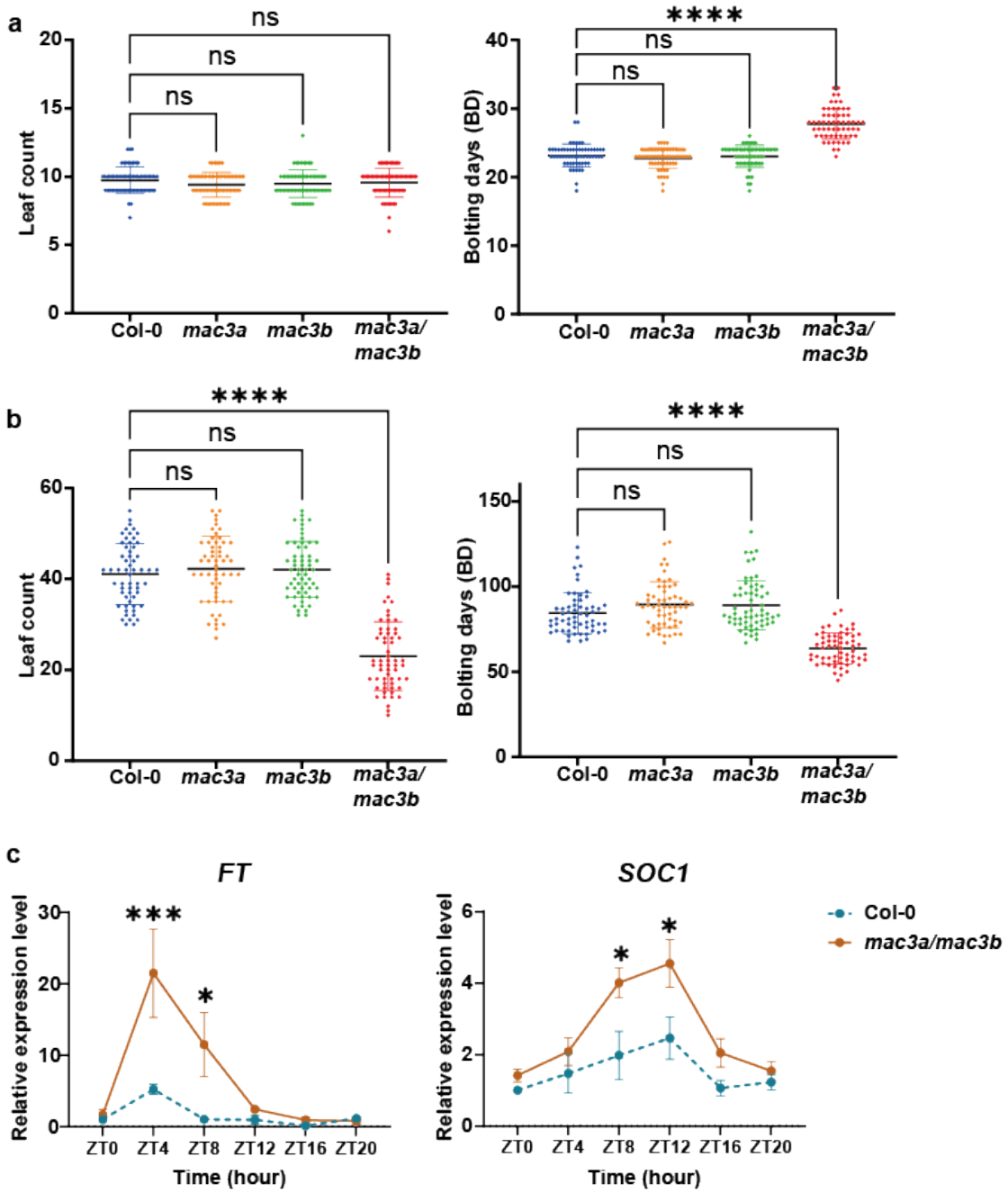

Figure 1. The flowering phenotypes of Col-0, *mac3a*, *mac3b*, and *mac3a/mac3b* mutants in long-day (LD) and short-day (SD)

The flowering time of Col-0, *mac3a*, *mac3b*, and *mac3a/mac3b* mutants grown under **(a)** LD (16h light/8h dark) or **(b)** SD (8h light/16h dark) was measured by rosette leaf number (left panel) when inflorescence reached 7 cm and bolting day (right panel) when inflorescence reached 1 cm. Data were collected from three biological replicates (n≥ 56) and analyzed using ANOVA and Kruskal-Wallis test: ****, p< 0.0001; ns, not significant. The numeric data can be found in Supplemental Table s1. **(c)** The transcript levels of *FT* (left panel) and *SOC1* (right panel) of Col-0 and *mac3a/mac3b* seedlings in SD. The samples were harvested every 4 hours after light on (Zeitgeber time 0, ZT0), and the expression levels were measured by RT-qPCR. The relative expression levels were normalized with *UBQ10* and compared to the Col-0 at ZT0. The error bars indicated standard deviations from three biological replicates. Data were analyzed using two-way ANOVA and Šídák's test: ***, p< 0.001; *, p< 0.05.

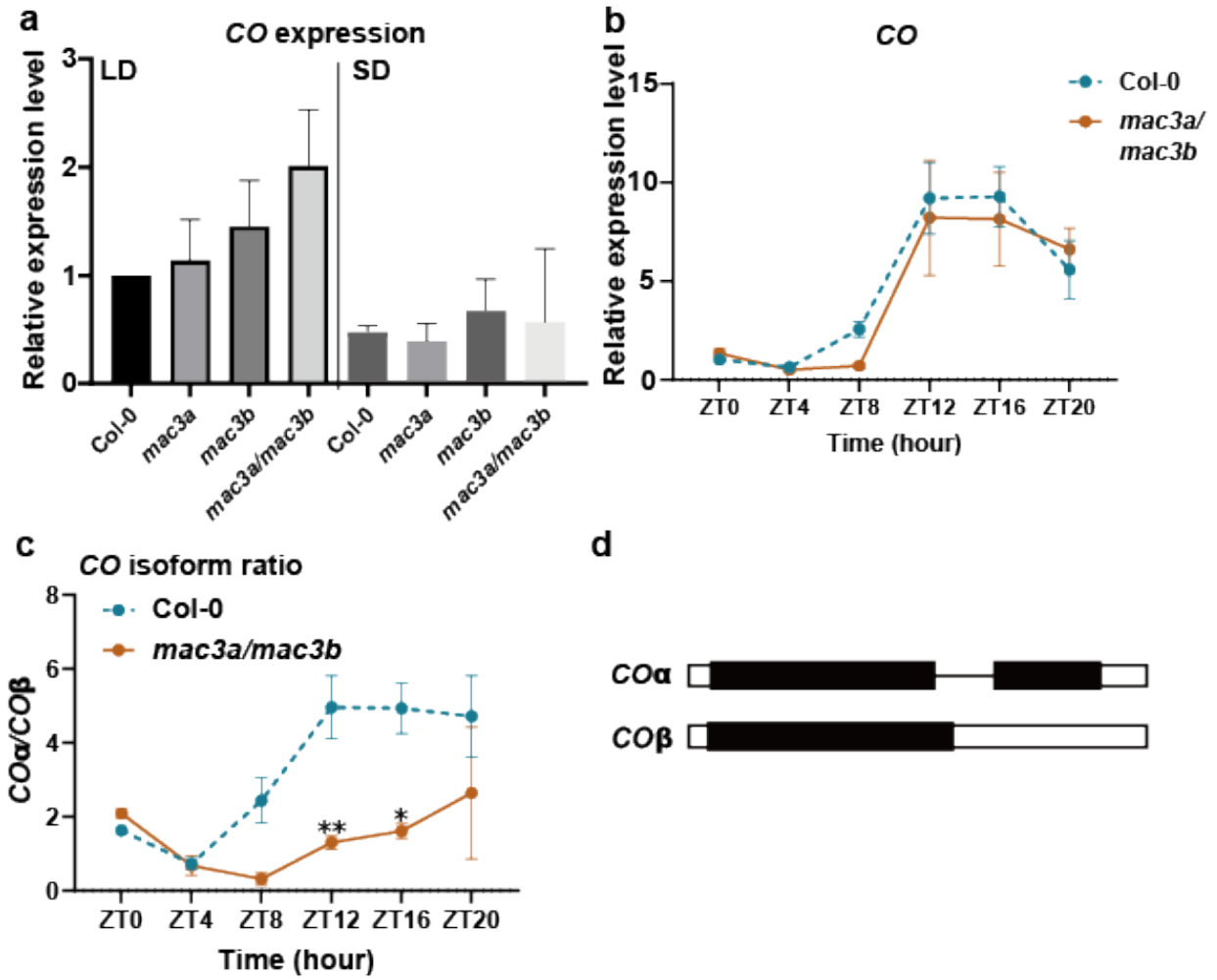

Figure 2. The expression of *CO* and its isoforms measured by RT-qPCR

(a) The relative transcript levels of *CO* in Col-0, *mac3a*, *mac3b*, and *mac3a/mac3b* mutants harvested at ZT16 under LD (16h light/8h dark) and ZT8 under SD (8h light/16h dark). **(b)** The relative diurnal transcript levels of *CO* in Col-0 and *mac3a/mac3b* mutants. The samples were harvested every 4 hours since dawn (ZT0). All time points were normalized with *UBQ10* expression and compared to the Col-0 sample at ZT0. **(c)** The ratios of *COα* over *COβ* in Col-0 and *mac3a/mac3b* mutants in SD. The expression of *COα* and *COβ* in Col-0 and *mac3a/mac3b* mutants can be found in Supplemental Figure s1. The error bars indicated standard deviations from three biological replicates. Data were analyzed using two-way ANOVA and the Šídák's test: **, $p< 0.01$; *, $p< 0.05$. **(d)** The diagram of transcript structure and the resulting protein isoforms of *COα* and *COβ*. The rectangles are exons, with the black-filled regions representing the protein-coding regions, and the line connecting them is the intron.

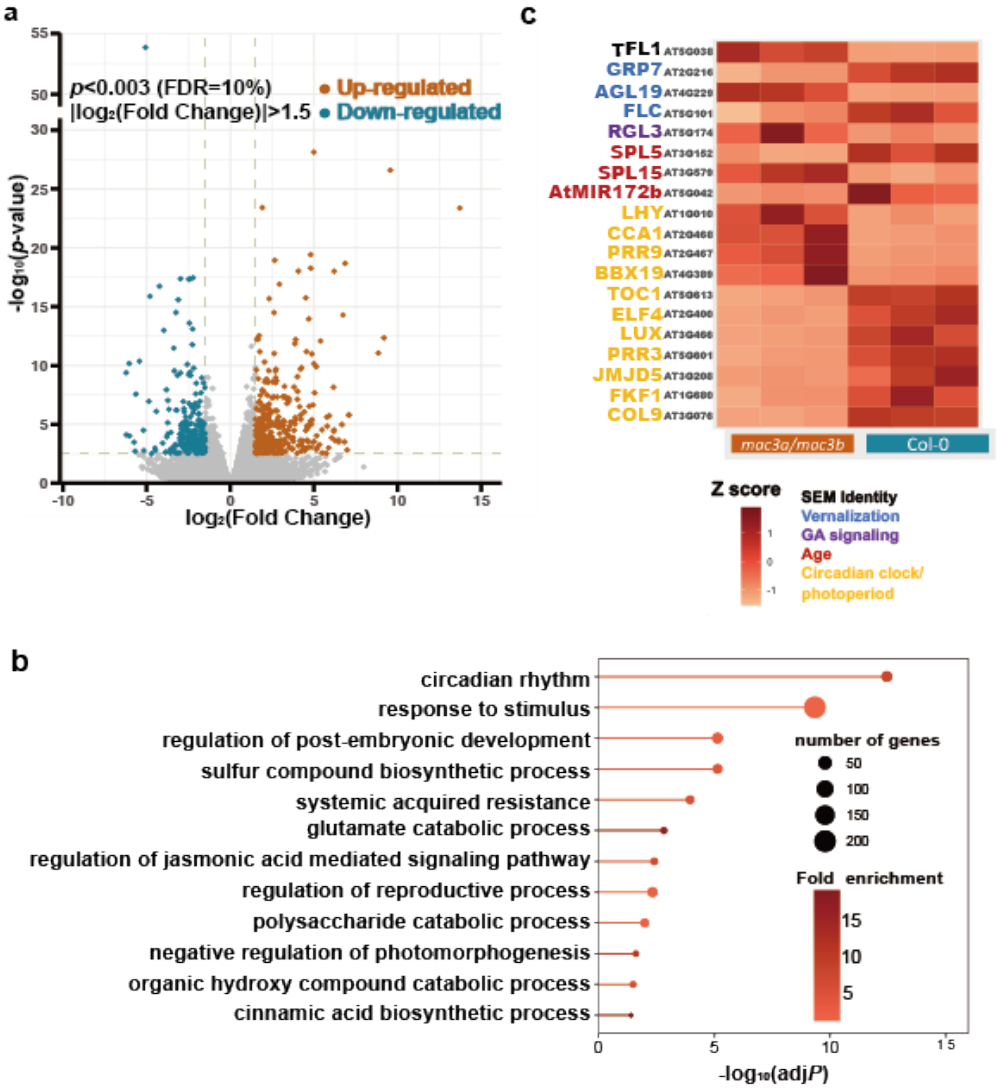

Figure 3. The differentially expressed genes (DEG) of SD-grown *mac3a/mac3b* mutant and their Gene ontology (GO) analysis

(a) The volcano plot of differentially expressed genes (DEG) in *mac3a/mac3b* mutants under SD compared to that in Col-0. The fold changes were calculated by comparing the means of normalized reads in three biological replicates of *mac3a/mac3b* and Col-0, and the p-values were calculated by T-Test of normalized reads. The up-regulated genes were marked in brown-orange, and the down-regulated genes were marked in blue with the criteria of $|\log_2(\text{fold change})| > 1.67$ and 10% FDR of accepted P values. The complete gene list is in Supplemental Table s2. **(b)** The top-ranked gene ontology (GO) of the biological processes category for the DEG. Selected GO terms were plotted on the lollipop plot, with gene numbers for each GO term in the DEG list represented by the dot size, and the darkness of the lollipops indicated the fold enrichment. The list of all GO terms was included in Supplemental Table s3. **(c)** Heat map of DEG genes involved in flowering regulation. The color represents the Z-score, calculated by the normalized gene expression reads between samples. The genes belonging to specific flowering pathways were color-coded. FDR: false discovery rate.

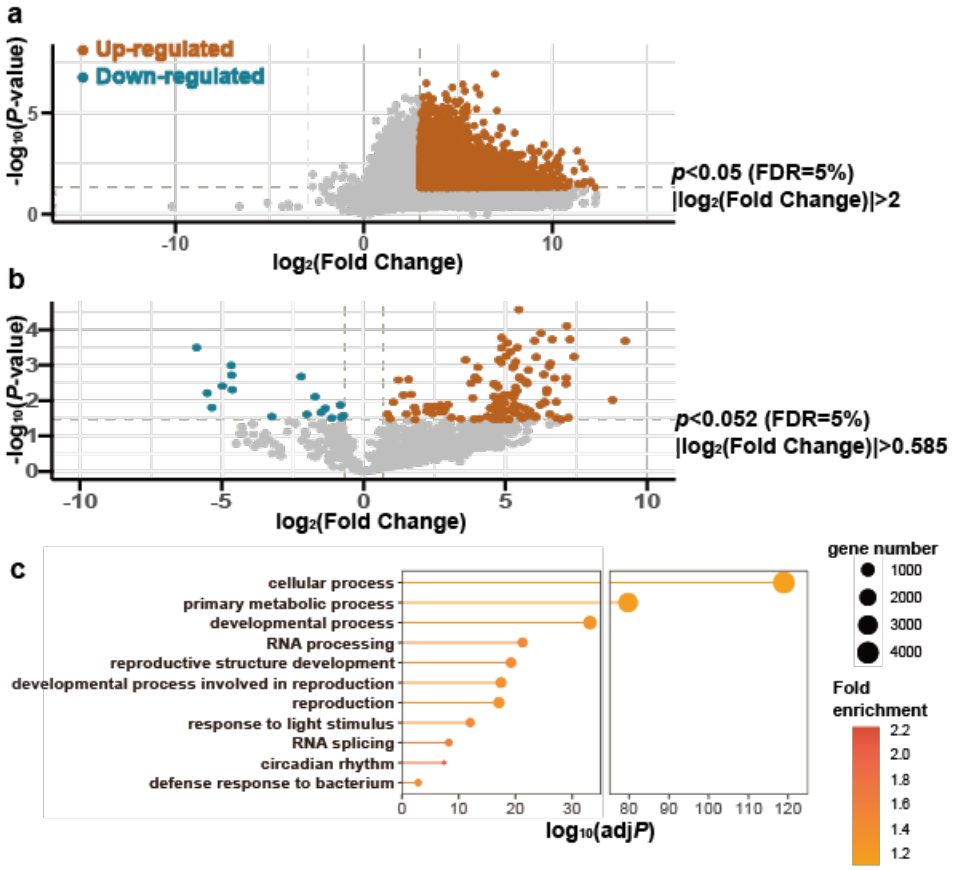

Figure 4. The differentially alternative spliced (DAS) events of SD-grown *mac3a/mac3b* mutant and their Gene ontology (GO) analysis

(a) The volcano plot of differentially intron retention (DIR) events between Col-0 and *mac3a/mac3b* identified by supporting reads ratio ($|\log_2(\text{fold change})| > 3$, FDR< 0.05). **(b)** The volcano plot of differentially exon skipping (DES) events between Col-0 and *mac3a/mac3b* identified by supporting reads ratio ($|\log_2(\text{fold change})| > 0.585$, FDR < 0.05). **(c)** The top-ranked gene ontology (GO) of biological processes for all differential alternative spliced events. Selected GO terms were plotted on the lollipop plot, with gene numbers exhibiting in the dot size and the darkness of the lollipops for the fold enrichment. The complete gene and GO lists were provided in Supplemental Tables s5-7. FDR: false discovery rate.

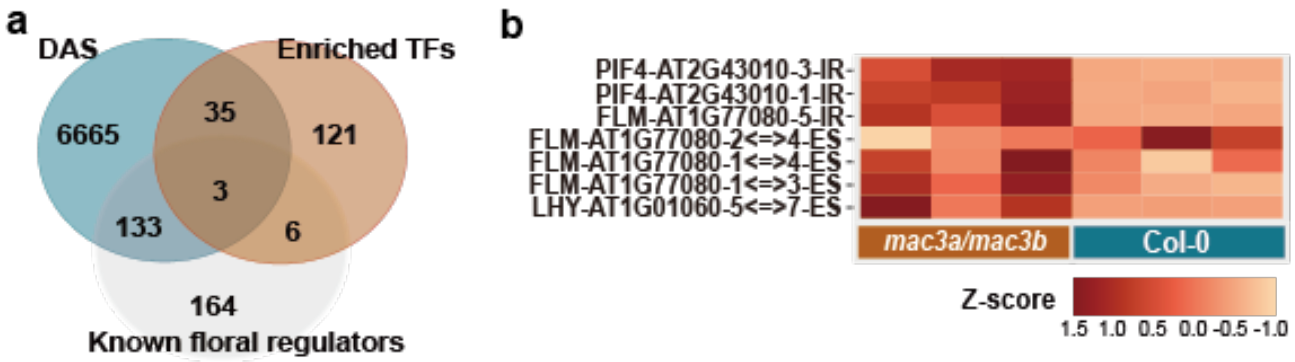

Figure 5. Identification of potential alternatively spliced targets of MAC3A and MAC3B for their flowering time regulation

(a) The Venn diagram represents the intersection of genes with differentially alternative spliced (DAS) events (Blue, Supplemental Tables s5-s6), the enriched transcription factors (TFs) upstream of the differentially expressed gene (DEG) (Orange, Supplemental Table s8), and known floral regulators (Grey, Supplemental Table s4). **(b)** Heatmap of *FLM*, *PIF4*, and *LHY* DAS events found in the *mac3a/mac3b*. The color represented the Z-score among samples from respective normalized values of splicing events. The label of each row refers to the gene name, TAIR ID, and the location of the event.

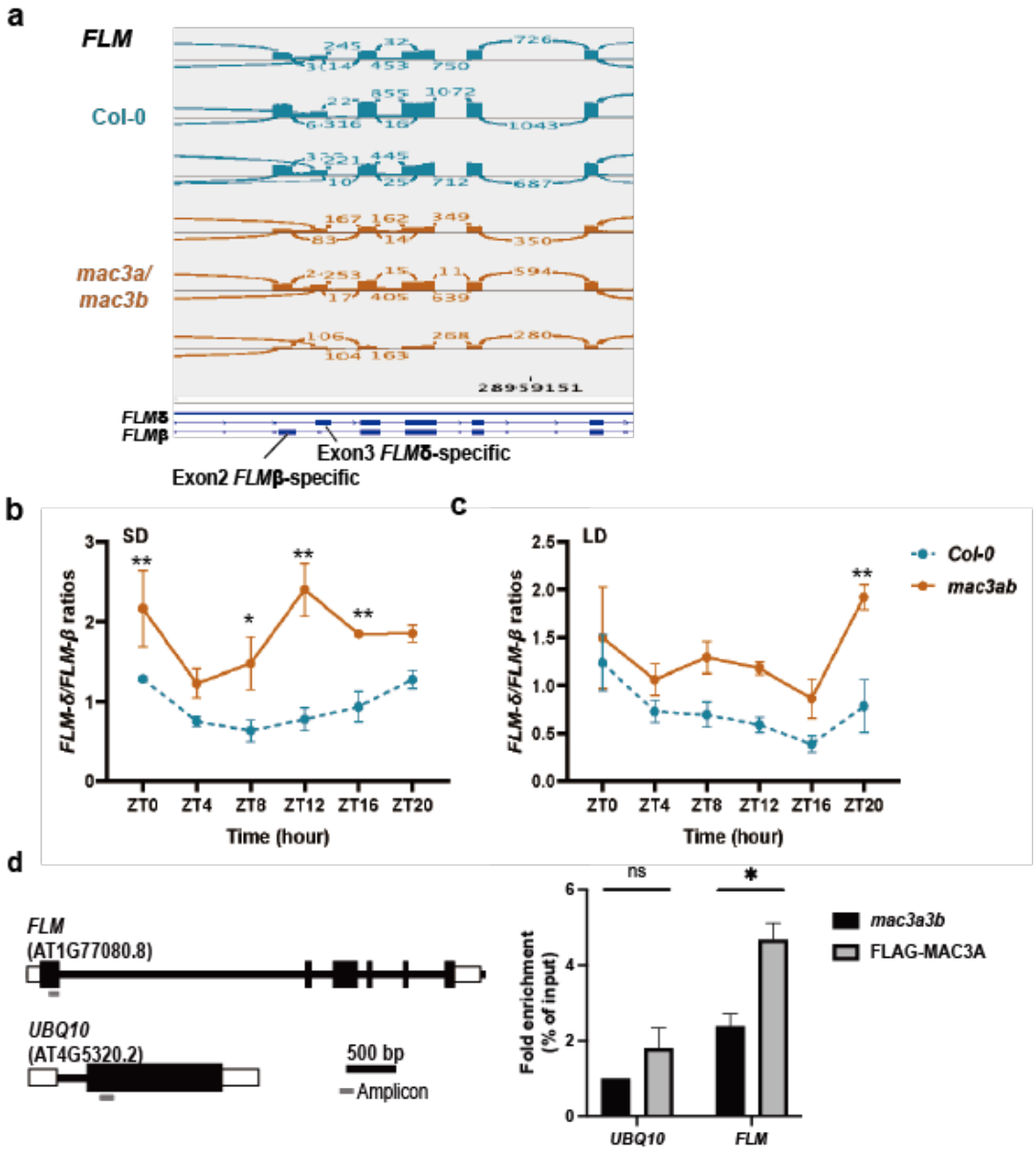

Figure 6. MAC3A and MAC3B directly regulate *FLM* splicing

(a) The sashimi plots on the *FLM* locus with highlighted exon2 and exon3 regions in Col-0 (Blue) and *mac3a/mac3b* (Orange). The height of the base represented the relative read depth, and the read number across junctions was shown between specific splicing junctions. The *FLMβ*-specific 2nd exon and *FLMδ*-specific 3rd exon were indicated. **(b and c)** The ratios of the *FLMδ* to *FLMβ* relative expression levels in the Col-0 and *mac3a/mac3b* in SD (b) and LD (c) were illustrated. The relative expression profiles were supplemented in Supplemental Figure s4. For each time point, the statistical analysis with a two-tailed t-test was performed (*P< 0.05 and **P< 0.01). **(d)** RNA-Immunoprecipitation followed by qPCR (RIP-qPCR) with anti-FLAG antibody in the FLAG-tagged MAC3A/*mac3amac3b* (FLAG-MAC3A) and *mac3amac3b* control. The *mac3a/mac3b* mutant and the transcript of *UBQ10* were used as control and negative control, respectively. The locations of the amplicons were illustrated in the *FLM* and *UBQ10* gene structure (left panel), and the locations of the amplicons were labeled underneath the gene structure. The enrichment of immunoprecipitated RNA was calculated relative to the input RNA and then compared to the value of *UBQ10* in the *mac3a/mac3b* mutant sample. The values shown are means ± SD. Statistical analysis was performed from three biological replicates using a one-tailed paired t-test (ns, non-significant, *P< 0.05).

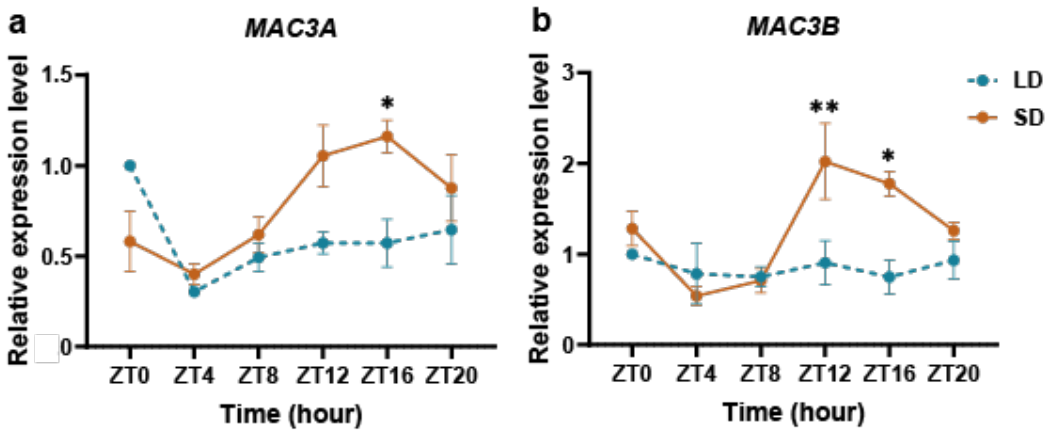

Figure 7. The expression of *MAC3A* and *MAC3B* in LD and SD measured by RT-qPCR

The relative diurnal expression pattern of *MAC3A* **(a)** and *MAC3B* **(b)** in LD and SD were measured with RT-qPCR. The expression was normalized with *UBQ10* and compared to the expression at ZT0 in LD. Error bars showed the standard deviations of three biological replicates, and the data were statistically tested using the two-way ANOVA and Šídák's test: **, $p < 0.01$; *, $p < 0.05$.

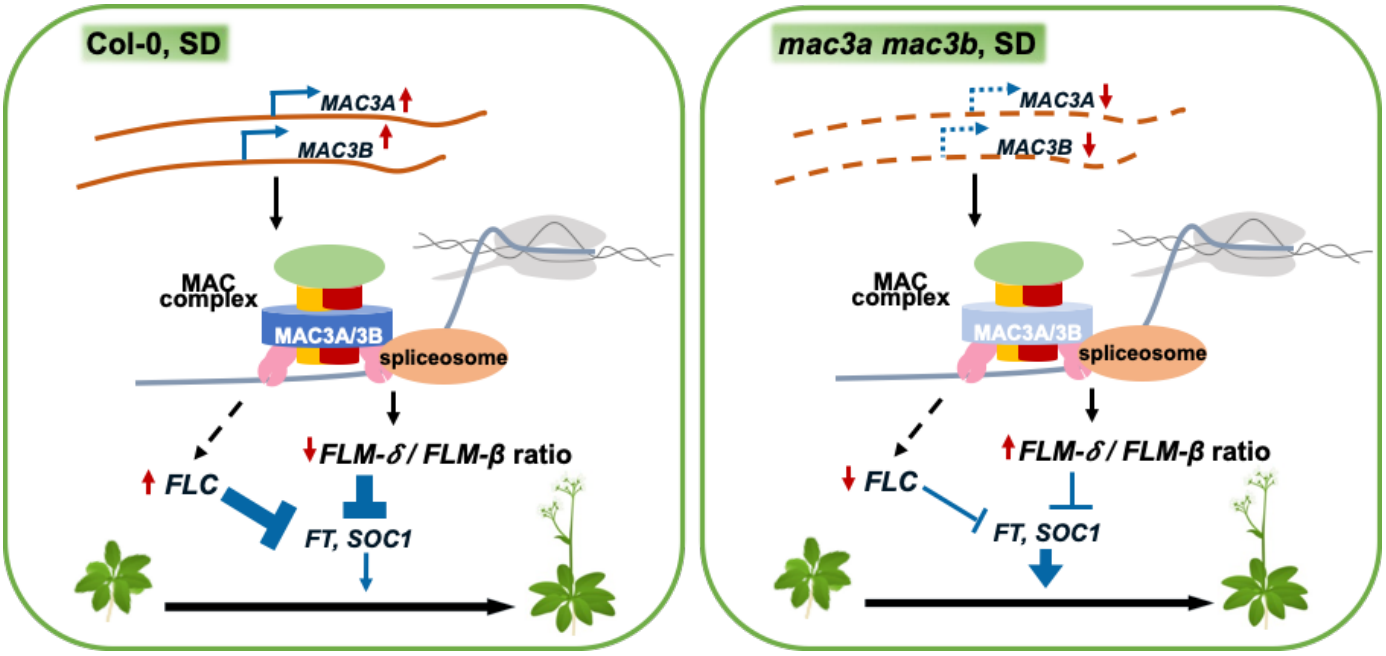

Figure 8. Proposed model of MAC3A and MAC3B mediated photoperiod signal to regulate flowering under SD

The working model of MAC3A and MAC3B repressing floral transition under SD. In Col-0, the expression of *MAC3A* and *MAC3B* transcription is upregulated under SD. MAC3A and MAC3B, potentially together with the MAC complex and spliceosome, facilitate proper RNA splicing of *FLM* through direct interaction. This maintains lower *FLMδ* to *FLMβ* ratios and represses floral integrators (*FT* and *SOC1*), thereby delaying the floral transition. Additionally, MAC3A and MAC3B are also required to maintain *FLC* levels to repress flowering under SD. In the *mac3a mac3b* hypomorphic mutant, reduced expression of *MAC3A/MAC3B* causes higher *FLMδ* to *FLMβ* ratios and decreased *FLC* expression under SD. Both changes increase *FT* and *SOC1* expression, resulting in early flowering.